Materials & Design 208 (2021) 109889

Contents lists available at ScienceDirect

Materials & Design

journal homepage: www.elsevier.com/locate/matdes

Modelling the influence of UV curing strategies for optimisation of inkjet based 3D printing

Peng Zhao [a,1], Yinfeng He [a,1], Gustavo F. Trindade [a,b], Martin Baumers [a], Derek J. Irvine [a], Richard J.M. Hague [a], Ian A. Ashcroft [a,*], Ricky D. Wildman [a,*]

[a] Centre for Additive Manufacturing, Faculty of Engineering, University of Nottingham, Nottingham NG8 1BB, United Kingdom
[b] Advanced Materials and Healthcare Technologies, School of Pharmacy, University of Nottingham, University Park, Nottingham NG7 2RD, United Kingdom

HIGHLIGHTS

- A predictive model is proposed to simulate the inkjet based 3D printing process.
- The model is validated using confocal Raman microscopy and shows predictability.
- A design framework is developed and used to determine and optimise quality.
- Optimised printing strategies' performance and cost-effectiveness are evaluated.

GRAPHICAL ABSTRACT

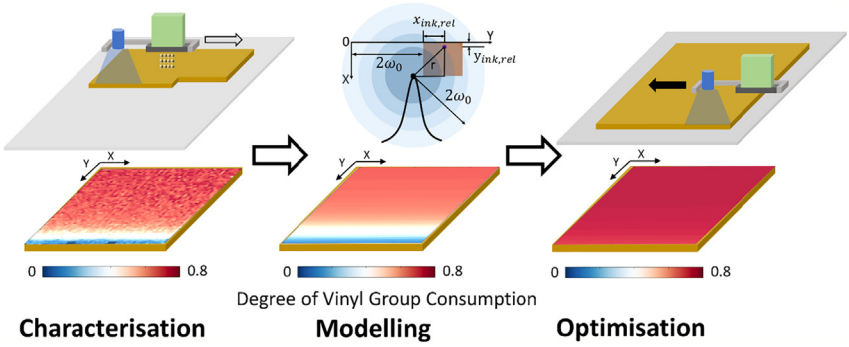

ARTICLE INFO

Article history:
Received 5 February 2021
Revised 17 May 2021
Accepted 8 June 2021
Available online 10 June 2021

Keywords:
Additive manufacturing
Inkjet printing
Polymerisation
UV light
Modelling
Optimisation

ABSTRACT

A predictive model is developed to assist in the design and manufacture of structures by inkjet based 3D printing (IJ3DP)/additive manufacturing. IJ3DP often exploits photopolymerisation to rapidly convert a photoreactive liquid ink into a solid product. Unfortunately, deviations from the intended design and product performance are often observed and a lack of understanding of the underlying processes and their interactions prevents users from resolving these issues. We develop and validate a predictive model that incorporates the critical processing parameters, including UV source pathway, UV intensity, printing strategy, and interlayer attenuation, such that we are able to predict the degree of ink conversion throughout the product. We show how this model can then be used to guide users by demonstrating the coupling of this description with a cost model and illustrating how printing strategy affects descriptors of both the quality and cost of production.

1. Introduction

Photoreactive materials have been widely used for the Additive Manufacturing (AM) of electronics [1–7], pharmaceutical devices [8–10] and implants [11,12]. The quality of the product is directly related to the level of photopolymerisation [13]. However, one difficulty of using photoreactive polymers is the lack of understanding and control over the level of photopolymerisation achieved during the manufacturing process. This can cause product performance issues, such as cytotoxicity [14,15], reduced mechanical performance [16,17] or application performance inconsistencies [17,18]. A commonly used optimisation methodology is to experimentally attempt a variety of processing parameters and ink formulations

* Corresponding authors.
E-mail addresses: Ian.Ashcroft@nottingham.ac.uk (I.A. Ashcroft), Ricky.Wildman@nottingham.ac.uk (R.D. Wildman).
[1] The authors contributed equally to this work.

https://doi.org/10.1016/j.matdes.2021.109889
0264-1275/

Nomenclature

A	area
B	absorbance
C	concentration
D	evaluation score
f	function
G	gap
k	rate constant
L	light intensity
l	length
n	number
Q	quality indicator
R	reaction rate
r	radius
s	position
t	time
V	vinyl group
v	moving speed
W	width
x	x direction/distance
y	y direction/distance
z	z direction/distance

Greek symbols

α	molar extinction coefficient
λ	UV radiation dose
τ	time
ϕ	quantum yield
χ	degree of vinyl group consumption
ω	Gaussian radius

Subscripts

0	initial condition/constant
A	attenuated
a	autoacceleration
I	printed point
i	initiation
L	one layer
l	light
n	the layer number
P	product
p	polymerisation
r	reaction
s	user-determined
t	termination
U	unattenuated
v	local element
x	x direction
y	y direction

[6,18–23] to determine the optimum production conditions iteratively. Adopting this strategy generally proves to be costly and time-consuming. Post-curing is another commonly used method to improve the level of polymerisation at the end of production. However, post-curing has limitations in some applications, such as: 3D printed tablets where the pre-dissolved drug can crystalise, leading to an opaque sample [9] which increases UV attenuation in post-curing; 3D print electronics where the degree of polymerisation of each dielectric layer is crucial, to avoid unwanted interaction between the conductive tracks and dielectric layers [24]; and high accuracy printing where uncured ink can lead to edge sagging effects, which affects the product's geometry accuracy [16]. Therefore, an alternative approach is to automate the print design process by carrying out theoretical studies and deploying predictive models [25–28], and use inverse methods to determine the optimal processing strategy with a minimum of experimentation.

The fundament of constructing such a predictive model is the relationship between UV dose and the level of photopolymerisation. The level of photopolymerisation is a function of the supplied energy dose (e.g. UV or laser beam) [25–27,29], quantum yield and absorption properties [30]. Predictive models have previously been developed for vat polymerisation processes in order to investigate the printability of the ink formulations [31,32], the level of photopolymerisation [33], and the product quality [34–36]. Both Emami and Rosen [34] and Li et al. [35] developed predictive models to optimise the dimensional accuracy of the cured features, considering the UV dose distribution and curing depth. By implementing a comprehensive reaction–diffusion model, Shusteff et al. [37] predicted the level of polymerisation within a holographic projection model and successfully optimised the process parameters to achieve micron-scale features. A more detailed model was built by Westbeek et al. [38], which predicted ink printability and specimen defects through multi-physics modelling of irradiation, conversion, mechanical solidification and chemical shrinkage. However, to the authors' best knowledge, a comprehensive study of the photopolymerisation in inkjet based 3D printing has not been carried out, which motivated the present study.

Compared with the vat polymerisation process, inkjet based 3D printing has a more complex and dynamic UV dosing strategy, which leads to localised processing defects. For example, to ensure the ink is cured as soon as it lands, a 'UV pinning' strategy is normally used especially for fine patterns, in which a UV unit is mounted to the printhead and moves with it, irradiating the ink as soon as possible after deposition [39,40]. However, during this process, instead of accurately delivering the UV dose according to the layered design, the moving UV unit repeatedly sweeps the whole printing platform, leading to repeated UV exposure to the developing printed structures. Additionally, the UV dose for each element is considerably different depending on its position and the print progression [16,17]. The element where the print starts receives far more UV dose than the element where the print finishes and leads to under cured bottom edge as well as a sagging effect [16]. In addition, because the UV light attenuation varies with time for each element, due to the moving UV light, the system kinetics also need to be taken into consideration in developing an accurate predictive model.

In light of existing photopolymerisation chemical kinetics studies, as well as their application to modelling the level of conversion in vat polymerisation, we developed a new predictive model that not only considered chemical kinetics but also introduced a novel way to calculate the cumulative UV dose of each element under the dynamic UV scanning scenario during IJ3DP. Such a model can be further adapted to other printing and UV scanning strategies utilised in IJ3DP. By additionally implementing a cost model, we created a novel design framework that helps the user to optimise their printing strategy for both part quality and cost effectiveness.

2. Methodology

3D printing is a layerwise manufacturing technique that sequentially stacks layers of materials to form the final product

(Fig. 1a). This study commenced with assessing the ink polymerisation during the process of printing a single layer (Fig. 1b and c). At this stage, the ink polymerisation relies on direct UV exposure from the UV unit (Fig. 1d). This method was then extended to multilayer printing (Fig. 1e), where attenuation of UV by subsequently printed layers was also taken into account.

During a single layer printing (Fig. 1a), liquid monomer ink is selectively deposited onto the substrate swathe by swathe and coalesced to form a continuous film. As a UV pinning inkjet printing, the printing unit moves at a constant speed along the X direction to print a single swathe. The UV source was attached and moved with the printing unit to trigger photopolymerisation of the liquid monomer after each swathe. It then moves in the Y direction once each swathe has been printed. After the printing of each layer is completed, the whole unit moves upwards in the Z direction to maintain the standoff distance (i.e. the distance between the print head and the printing surface). By repeating this process, a 3D structure is achieved.

The kinetics of the UV initiated polymerisation and the UV dose accumulation per user-defined element ($0.1\ mm \times 0.1\ mm \times 0.01\ mm$ in this study) are the two core aspects of the model developed in this study. The study commenced by developing a predictive model, by deriving a relationship between the accumulated UV radiation dose and the level of photopolymerisation with consideration of the auto-acceleration effect [41]. A descriptive model is proposed to calculate the total accumulated UV dose for each element over the entire production period; the proposed model considers the spatial UV intensity distribution of the UV source, the time-dependent distance between the UV source and a specific element and light attenuation throughout the object based on a Gaussian UV beam profile [34,42,43] and the Beer-Lambert light attenuation law [44]. The multi-physics model derived enables prediction of the level of polymerisation that would be seen in each element following any print pattern; thus delivering a novel development for IJ3DP design optimisation and quality control.

2.1. Kinetics of UV curing during inkjet printing

Photopolymerisation is a type of free radical polymerisation process that is generally described in four stages: decomposition, initiation, propagation and termination. A photoinitiator (I) is initiated by a UV source to generate free radicals ($A\cdot$). These free radicals react with vinyl groups (V) to form a chain of large free radical molecules ($V_n\cdot$), which can then terminate into stable polymer chains. The process can be described using the following kinetic relations [45,46]:

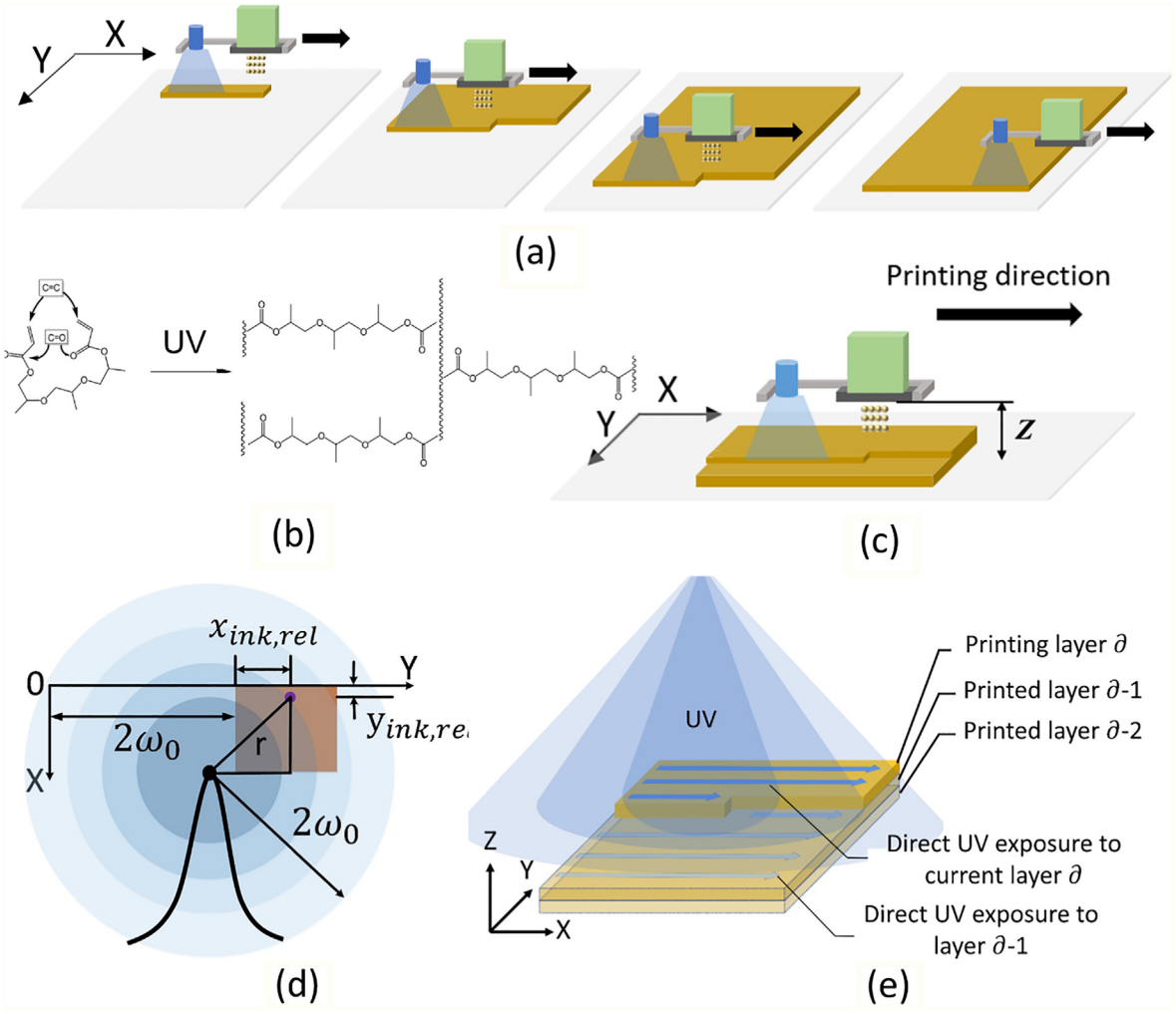

Fig. 1. Schematic of the inkjet-based additive manufacturing process and the models used: **a)** the standard printing process used to establish the model; **b)** photopolymerisation of TPGDA during the printing process; **c)** the printing of a component in a Dimatix DMP-2830 Inkjet printer; **d)** UV radiation intensity distribution in X-Y planar; **e)** UV radiation distribution during multilayer printing.

Decomposition:

$$I \xrightarrow{k_d} 2A\cdot \tag{1}$$

Initiation:

$$A\cdot + V \rightarrow AV\cdot \tag{2}$$

$$R_i = 2fk_d[I] = 2.3\phi_i\alpha_i[I]L(t) = 2k_iL(t) \tag{3}$$

Propagation:

$$V_n\cdot + V \xrightarrow{k_p} V_{n+1}\cdot \tag{4}$$

$$R_p = -\frac{d[V]}{dt} = k_p[V][V\cdot] \tag{5}$$

Termination:

$$V_n\cdot + V_m\cdot \xrightarrow{k_t} terminated\ polymer\ chain \tag{6}$$

$$R_t = 2k_t[V\cdot]^2 \tag{7}$$

where I is the reagent initiator molecule, A is the decomposition product radical, k_d is the rate constant of decomposition. f is the efficiency of the initiator i.e. the radicals reactivity to the monomer, which is typically $0.3 - 0.8$ for thermolysis. R_i, R_p and R_t are the initiation, propagation and termination rate respectively andk_i, k_p and k_t are their respective rate constants. ϕ_i is the initiation quantum yield, α_i is the molar extinction coefficient of the photoinitiator, $[I]$ is the photoinitiator concentration, $L(t)$ is the light intensity, t is time, $[V\cdot]$ is the radical concentration and $[V]$ is the vinyl group concentration. In practice, there are two types of termination mechanism, defined as combination and disproportionation. In this study, as both are dependent on two radicals meeting, they have been represented in this single general equation. Details of the termination mechanism are described in Supplementary Section 10.

Within this study, it was assumed that; (a) k_p and k_t are independent of the size of the initiator radical and are constant throughout the processing event when using a specific monomer/-combination of monomers and (b) a steady-state assumption, which defines the net rate of free radicals production as zero, i.e. the initiation and termination rates are equal [45]. Therefore, the initiation rate can be expressed as [45],

$$R_i = R_t = 2k_t[V\cdot]^2 \tag{8}$$

After substitution of Eqs. (3) and (8) into Eq. (5), the photopolymerisation rate is obtained,

$$R_p = -\frac{d[V]}{dt} = k_p[V]\left(\frac{k_iL(t)}{k_t}\right)^{1/2} \tag{9}$$

After integration of Eq. (9) and further simplifications, the vinyl group consumption is defined as,

$$\chi_p = 1 - \frac{[V]}{[V]_0} = 1 - e^{k_{r,p}\lambda} \tag{10}$$

where $k_{r,p}$ is defined as below:

$$k_{r,p} = -k_p\frac{k_I^{1/2}}{k_t^{1/2}} \tag{11}$$

λ is UV radiation dose, defined by

$$\lambda = \int_0^t L^{1/2}(t)dt \tag{12}$$

In this study, the curing process is a free radical bulk polymerisation process with no diluent, and so all the material can potentially participate in the reaction to form the final product [46]. In this situation, a higher polymerisation rate is often evident, since the reaction is exothermic and the medium progressively increases in viscosity as the reaction proceeds. Thus the increase in temperature and reduced mass/heat transfer within the medium leads to a local temperature rise, in the extreme case of this process, the reaction will auto-accelerate (also known as the Trommsdorff–Norrish effect). To accommodate this, the kinetic model developed by Jaso *et al.* was adopted [41]. This kinetic model is comprised of two sub-models, one is the classical theory of free radical polymerisation, and the other describes the autoacceleration effect. The polymer concentration is introduced as an extra factor to describe the auto acceleration [41]. We applied this kinetic model to the photon-triggered free-radical bulk polymerisation, thus the photopolymerisation rate at the autoacceleration stage can be expressed as:

$$R_a = -\frac{d[V]}{dt} = k_p[V][V\cdot] = k_{pa}[V]\left(\frac{k_iL(t)}{k_t}\right)^{1/2}\cdot[R] \tag{13}$$

where $[R]$ is the reacted vinyl group concentration, k_{pa} is the rate constant of auto-acceleration. Through the integration of Eq. (13) and further simplifications, the degree of vinyl group consumption at the autoacceleration stage is defined as,

$$\chi_a = \frac{1}{1 + e^{k_{r,a}\ (\lambda - \lambda_C)}} \tag{14}$$

where λ_C is the required UV radiation dose to achieve half of the maximum degree of vinyl group consumption at the autoacceleration stage. $k_{r,a}$ is the constant for the autoacceleration stage,

$$k_{r,a} = -k_{pa}\frac{k_i^{1/2}}{k_t^{1/2}} \tag{15}$$

The total degree of vinyl group consumption of the bulk polymerisation consists of two parts: (a) classical theory of free radical polymerisation, and (b) autoacceleration theory [41], leading to,

$$\chi = \chi_p + \chi_a \leq 1 \tag{16}$$

Additionally, the polymerisation rate is limited by the diffusion capability of both the free radicals and the monomer as the reaction progresses. Both of these factors will change at a higher degree of vinyl group consumption [47]. The free movement of free radicals and monomer becomes more difficult with the increasing viscosity caused by polymerisation. Hence, both the classical free radical polymerisation and the autoacceleration polymerisation models have a maximum degree of vinyl group consumption that can be achieved [48–50], i.e. in the extreme case the steady state assumption breaks down. Therefore, we introduce the maximum degree of vinyl group consumption as a correction factor, which is expressed as follows,

$$\chi = \chi_{max,p}\left(1 - e^{k_{r,p}\lambda}\right) + \frac{\chi_{max,a}}{1 + e^{k_{r,a}\ (\lambda - \lambda_C)}} \tag{17}$$

where $\chi_{max,p}$ and $\chi_{max,a}$are the maximum degrees of vinyl group consumption that can be achieved by the classical free radical polymerisation and the autoacceleration polymerisation respectively. Details of the predictive model derivation are described in Supplementary Section 11.

2.2. Dynamic UV dose accumulation per element during production

The amount of UV exposure that each element experienced during processing varied depending on its specific illumination conditions. To accommodate this, the proposed model accounts for the history of exposure throughout the printing process. We started with a 2D model that considered a single layer printing process. The 2D model was then extended to 3D by considering the extra

UV exposure in existing layers as subsequent layers of ink are deposited. During this process, the UV source was elevating in the Z direction as layers stacking up, so the distance to the UV source is changing for each layer.

As shown in Fig. 1d, on the basis of observation, we defined UV light illuminating area was always more extensive than the printing area of each swathe. Therefore, the UV light will deposit extra UV energy onto the ink printed in a previous swathe, which will initiate further polymerisation of the monomer of deposited ink. After a designed layer has been completed, the following layer will be printed on to it.

Various light intensity distribution profiles such as linear, circular, quadratic and Gaussian have been used in other studies to simulate the light distribution [51]. In this case, a Gaussian beam profile was used [52,53] and so the UV light intensity profile is defined as [42,43],

$$L(t) = L_0 f(t) = L_0 exp\left(-\frac{2r^2(t)}{\omega_0^2}\right) \tag{18}$$

where L is the light intensity, L_0 is the peak intensity,$f(t)$ is a Gaussian function, r is the radial coordinate of distance from the centre of the beam, ω_0 is the radius at which the intensity values fall to $1/e^2$ of its value on the axis, and the intensity is 0.0003 of its peak value at $2\omega_0$ or twice the Gaussian radius.

It was assumed that there were negligible surface reflectivity, non-reactive scattering and no diffraction during photoreaction doing the processing. Additionally, the exact radial coordinate of the distance between the centre of the beam and the printed point was calculated to estimate the light intensity of a printed point at any time (Fig. 1d). Details are described in Supplementary Section 3.

During a multilayer printing process, the instantaneous photochemical reaction and the light propagation of the printed ink also have to be taken into consideration. Light will penetrate and reach the previously printed layer that will lead to further polymerisation. The Beer-Lambert law was used to describe the relationship between the attenuation of the travelling light and the characteristics of the subsequent reaction and thus properties of the material [44].

$$B = log_{10}\left[\frac{L_0}{L(z,t)}\right] = z[\alpha_r C_r(z,t) + \alpha_P C_P(z,t) + \alpha_m C_m(z,t)] \tag{19}$$

where B is the absorbance of the sample; I_0 is the peak intensity, $L(z,t)$ represents the light intensity at a depth z below the irradiated surface z_0 and at the time t; $C_r(z,t)$ are the concentrations of reactants, $C_P(z,t)$ are that of products and $C_m(z,t)$ are that of an inert medium, α_i $(i = r, P, m)$ are the respective molar extinction coefficients, and t and z refer to time and location along the light direction, respectively.

In this study, the UV light attenuation through the printed ink was found to be negligible when measured by a UV–vis spectrometer (Supplementary Section 4). On the basis of this observation, we assume that the photoinitiator concentration in this study is low and will not cause UV light attenuation. There is also no inert medium in the ink, so we assumed that all the UV light attenuation was caused by the polymerised monomer. The value of α_P was obtained by measuring the equivalent UV–Vis absorbance of different printed layers, the methods by which this was achieved are shown in Fig. S2 in Supplementary Section 4 and in Section 2.4. The attenuated light intensity was simplified to be,

$$L(z,t) = L_0 f(t) \cdot 10^{-z \cdot \alpha_P C_P(t)} \tag{20}$$

The UV radiation dose at the *nth* layer is expressed as,

$$\lambda_n = \int_0^t L^{1/2}(z,t)dt = L_0^{1/2} \int_0^t f^{1/2}(t) 10^{-1/2 \cdot z \alpha_P C_P(t)} dt \tag{21}$$

In multilayer inkjet printing, the typical standard jetting and UV radiation process procedures are to progress from the first swathe to the last swathe across a layer and from the bottom layer to the top layer in building the Z height, as shown in Fig. 1a and 1e. In this study, a new description of the effect of UV dose attenuation was applied: every layer of printed ink here is considered to be transparent to UV light before polymerisation. The UV light will attenuate when travelling through each layer once the ink is solidified. Each time a fresh layer is deposited on top of an existing one, the existing layer will start with being directly exposed to UV light until being gradually covered by the fresh layer. From this point and afterwards, the UV light that reached the existing layer will be attenuated (e.g., *Layer 2* in Fig. S3). By taking these into consideration, the total UV radiation dose λ_n of any printed point at layer n can be estimated as (Fig. S3 and Supplementary Section 5),

$$\lambda_n = \lambda_U + \sum_{n-1}^{1} \lambda_{A,n-1} \tag{22}$$

where λ_U is the full X-Y planar of unattenuated UV radiation dose, λ_A is the attenuated UV radiation dose. Details of UV radiation dose calculation for different layers are shown in Supplementary Section 5.

2.3. Determination of key model parameters for a specific ink formulation

To apply the model to an actual printing process using a specific ink formulation, it was necessary to determine a set of parameters related to the polymerisation kinetics and the UV attenuation before and after polymerisation. In this study, the ink formulation comprised of tripropylene glycol diacrylate (TPGDA, 99 wt%, technical grade purchased from Sigma-Aldrich, $\geq$ 82.5% purity, which is a mixture of isomers, which contained MEHQ and HQ as inhibitors) as the structural monomer, and 2, 2-Dimethoxy-2-phenylacetophenone (DMPA, 1 wt%, $\geq$ 98.5% purity, Sigma-Aldrich) as the photoinitiator. TPGDA [54] and DMPA [55] are assumed to have negligible absorbance at the illumination wavelength of 365 nm on the basis of UV–vis spectrometer measurements before polymerisation (Supplementary Section 4). Therefore, the concentration of the unreacted/undecomposed components of these reagents left in the mixture did not need to be taken into consideration when calculating UV attenuation. By measuring the ink residual reagent distribution (i.e. level of cure) and absorbance at the UV source wavelength within a specimen, it was possible to extract the model coefficients needed to predict the conversion to polymer achieved for this selected ink, under a range of printing conditions. The model was then validated by printing and analysing specimens under various different printing conditions, including differing UV intensity levels and printing strategies.

The photopolymerisation of TPGDA is shown in Fig. 1b. The printing was carried out using a Fujifilm Dimatix DMP-2830 material printer contained within a glovebox contains an inert dinitrogen atmosphere. This environment was chosen to eliminate the oxygen inhibition effect during the polymerisation. The schematic of the machine set up is shown in Fig. 1c. The printing unit consists of a printhead and a UV illumination unit, which moves as a whole in the X (printing) direction. Photoreactive ink droplets were deposited onto the substrate by the printhead located at the centre of the unit. The UV unit next to the printhead scanned across the printed area following the printhead. The UV energy triggered the photopolymerisation process to convert the liquid monomer ink to a solid. The fixed distance between the UV unit and printhead was 45 mm, and the standoff distance between the substrate and the printhead was 1 mm. All the printing was carried out with

three nozzles, at 3 kHz jetting frequency and a 30 μm droplet spacing. Further printing details are shown in Table S1 in Supplementary Section 1. An acetone-treated silicon dioxide/silicon wafer was selected to be the substrate since it was found to offer reliable droplet formation and coalescence in pre-trials. The UV unit had a wavelength of 365 nm and a measured maximum light intensity at a 1 mm standoff distance of 1245 W/m^2. The relation of UV level to UV light intensity is shown in Supplementary Section 2.

2.4. Tracking the distribution of vinyl group to assess element polymerisation

To experimentally determine the spatial distribution of the residual vinyl group concentration, single and multilayer samples (5 mm × 5 mm per layer) were printed and subjected to analysis by confocal Raman microscopy using a Horiba LabRAM HR confocal Raman microscope with a motorised X-Y-Z stage. All Raman data were produced using a 532 nm laser (at a power of 129 mW), a 100× objective lens and over the range 1047–1555 cm^{-1}. Spectra were acquired using a Synapse CCD with 1024 pixels. The instrument was calibrated using a standard Si (1,0,0) reference band at 520.7 cm^{-1}.

X-Y maps of the single-layer samples were obtained with a 500 μm confocal hole by collecting spectra in 100 μm steps across a 5250 × 5250 μm^2 region, totalling 2916 spectra per sample. Each spectrum was obtained for 2 s with two accumulations each. The optimal height for each point was determined *a priori* using the autofocus function of the instrument. Z profiles of the multilayer samples were obtained with a 50 μm confocal hole by collecting spectra in 2.5 μm steps. Each spectrum was collected for 40 s with two accumulations each. Besides mapping single and multilayer samples, single-point measurements of the uncured TPGDA monomer with 1 wt% photoinitiator were acquired with an acquisition time of 200 s with two accumulations.

The normalised degree of unreacted vinyl domains was extracted from the Raman data using an automated routine written in a MATLAB script to measure the relative consumption of vinyl groups (represented by the *C = C* band at 1639 cm^{-1}): Each spectrum was background-removed, and the areas *A* under the *C = C* (1639 cm^{-1}) and *C = O* (1723 cm^{-1}) peaks were measured. The relative vinyl group concentration $[V]/[V]_o$ was then calculated, for a given spectrum, by:

$$\frac{[V]}{[V]_0} = \frac{\left(\frac{A_{C=C}}{A_{C=O}}\right)}{\left(\frac{A_{C=C}}{A_{C=O}}\right)_0} \tag{23}$$

where *0* stands for the spectrum of unreacted ink. A Raman reference spectrum is shown in Supplementary Section 6. It should be noted that the level of residual vinyl groups will never reach zero. This is because the functional monomer is a difunctional monomer, i.e. it contains two reactable acrylate groups. The polymer formed will be a 3-dimensional, branched, cross-linked network, as the monomer can react twice to link two independently growing chains together. Thus, after a certain size has been reached the polymer structure will not have the mobility to enable all the second acrylate functions to find another monomer/chain to react with and so they will remain unreacted even if all the monomer is consumed. Prior publications found that for diacrylate monomers, there is a conversion limit of $\sim 80\%$, that matches our experimental observations [48,50]. This is mainly due to the free movement of free radicals and monomer becomes more difficult with rapid increasing viscosity caused by polymerisation. The thickness of a single layer of TPGDA was 0.01 mm in this study (as shown in Table S1). As the depth of the specimen increases the attenuation increases, and the received peak signal measured at that depth will reduce and approach the amplitude of the noise signal. Therefore we chose ten layers (100 μm), as this is the maximum thickness for which this method can resolve data before attenuation significantly depletes the signal.

2.5. Cost model for inkjet printing

To evaluate the performance of a printing strategy, the quality and cost [56,57] of the printed parts were both considered. Since the quality of an inkjet-printed part is closely correlated to the satisfactory level of ink conversion [16], we introduce a user-determined threshold for the degree of vinyl group consumption χ_s, which can represent the level of ink polymerisation, this also takes into account the caveat above. Elements that were above this threshold were counted as acceptable quality (= 1), where those below it were counted as unacceptable (= 0) (Eq. (25)). A quality control indicator *Q* was then defined as the ratio between elements with acceptable quality and all the elements,

$$Q(\%) = \frac{\sum_1^n D}{n} \times 100\% \tag{24}$$

$$D = \begin{cases} 0, (\chi_v < \chi_s) \\ 1, (\chi_v \geq \chi_s) \end{cases} \tag{25}$$

where n is the total number of elements in the sample, χ_v is the local degree of vinyl group consumption in an element, χ_s is a user-determined threshold of the degree of vinyl group consumption and *D* is the evaluation score.

The value of the quality indicator depends on the user's expectation of quality control. A higher value of the quality indicator means the product quality was closer to the user's expectation. A cost model for additive manufacturing [58–60] was found to be complicated to calculate, with a number of different cost categories, including machine indirect cost, non-machine indirect cost, labour, material and energy consumption [58]. The machine indirect cost is dependent on both machine cost rates and usage times. Non-machine indirect costs are dependent on the cost rates of infrastructures and overheads and the processing times. Researchers have simplified the cost model to a few main factors, such as raw material cost and printing cost [61–65]. By analysing and comparing the cost factors for different printing strategies, we find that the main difference is the build time in this study. Therefore, in this work, only the build time is considered to access the cost of different printing strategies. The total build time t_{build} is calculated as [58],

$$t_{build} = (t_x + t_y + t_0) \times n_l \tag{26}$$

where t_x is the time required for X-axis movement of a single layer, t_y is the time required for Y-axis movement of a single layer, t_0 is the time needed for the movement of printhead from the idle position and n_l is number of layers. Details of the calculation are given in Supplementary Section 9.

3. Results and discussion

3.1. Parameters determination and model validation

This section details how the parameters of the model were determined using the measured vinyl group consumption data for both a printed single, individual layer and multilayer samples, using the highest UV intensity of 1245 W/m^2. As the highest UV intensity was used, the data covered a UV dose range $(3.46 - 1328.63(kg/s)^{1/2})$ and monomer conversion range $(0.12 - 0.78)$. Further samples were then prepared using lower UV light intensities (1019, 832 and $538 W/m^2$) to validate these

experimentally determined parameters. An element size independency study was performed, to check the sensitivity of the predictions with respect to the size of element used to calculate the photopolymerisation physics, and is presented in Supplementary Section 12. It was determined that, for the physical attributes of the printer set up being modelled in this study, an element size of 0.1 mm (3 droplets) × 0.1 mm (3 droplets) × 0.01 mm (1 droplets) was sufficient, and further reductions in element size did not produce significant changes in the predictions. For other printer configurations, the optimal element size may be different, hence a new element size independency study is recommended for each printer configuration.

Fig. 2a shows the distribution map of measured vinyl group consumption for a single layer obtained by Raman microscopy. When a square sample was printed with UV intensity of 1245 W/m^2, starting from the top left corner and ending up at the bottom right, the degree of vinyl group consumption was found to vary in the Y direction while it remained relatively constant in the X-direction. The consumption gradient was noted to match the UV dose prediction in Fig. 2c, where the ink that was deposited at the end of the printing area will have received the lowest UV dose ($3.46(kg/s)^{1/2}$) resulting in lower vinyl group consumption (0.12 at the lowest UV dose compared with 0.70 at the highest UV dose).

The degree of vinyl group consumption in the Z-direction under the same UV intensity is shown in Fig. 2b. The Z-axis origin is set at the top of the printed sample. The degree of vinyl group consumption at the bottom (0.77) is much higher than the top layer (0.69) due to the fact that the bottom layer was continuously exposed to UV when subsequent layers are printed on top. The degree of vinyl group consumption at the bottom is close to the maximum

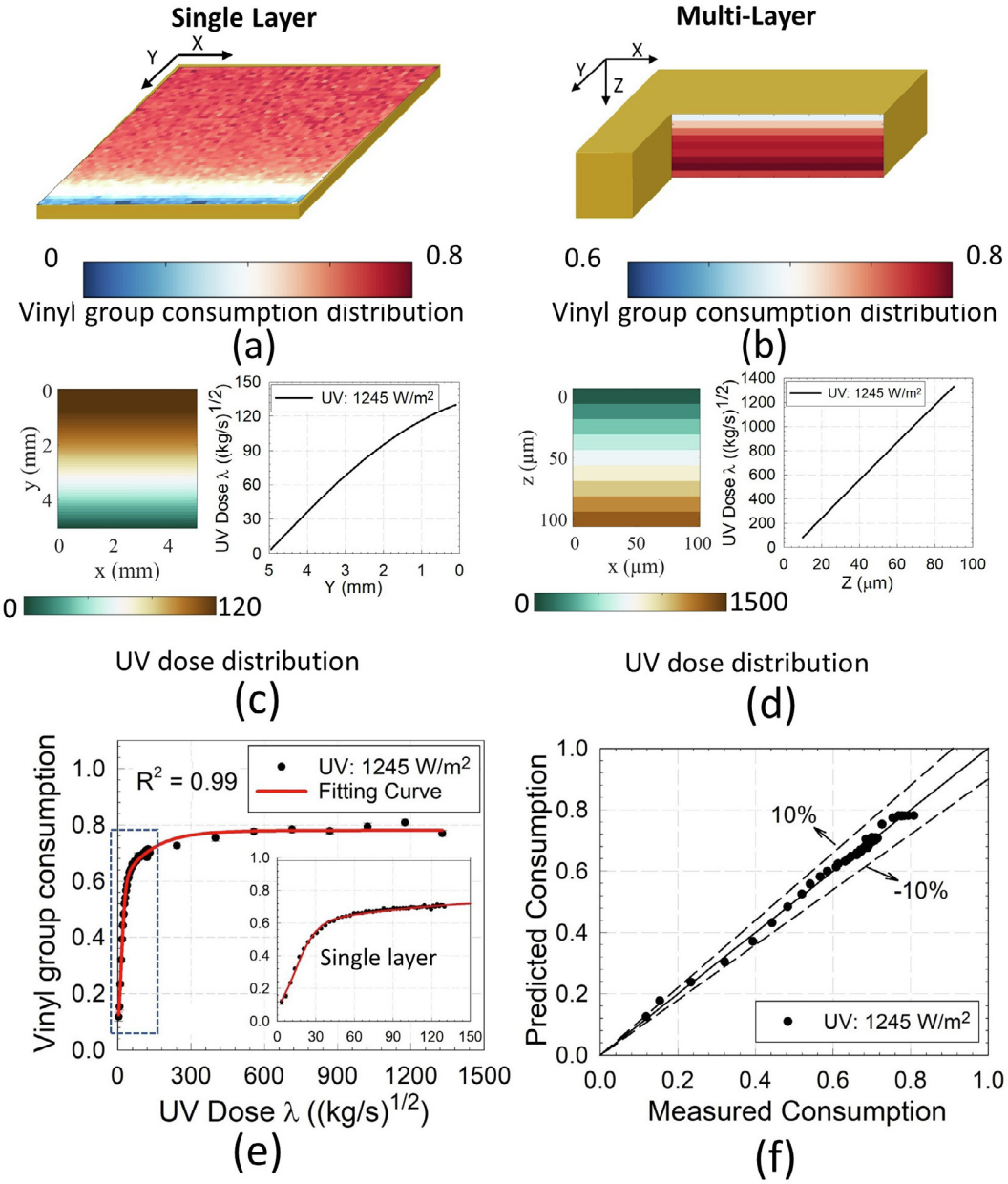

Fig. 2. Predictive model parameters are determined on the basis of vinyl group consumption data measured by Raman microscopy, the chosen specimen is printed under 1245 W/m^2 UV intensity: **a)** measured distribution of vinyl group consumption within a single layer; **b)** measured distribution of vinyl group consumption through multilayers; **c)** calculated distribution of UV radiation dose within a single layer; **d)** calculated distribution of UV radiation dose through multilayers; **e)** degree of vinyl group consumption data with the best fitting curve; **f)** deviation assessment of the predictive model.

Table 1
Fitted parameters for Eq. (17).

Parameters	$\chi_{max,p}$	$\chi_{max,a}$	$k_{r,p}$	$k_{r,a}$	λ_C
Value	0.2079	0.5729	−0.0083	−0.1258	14.0719

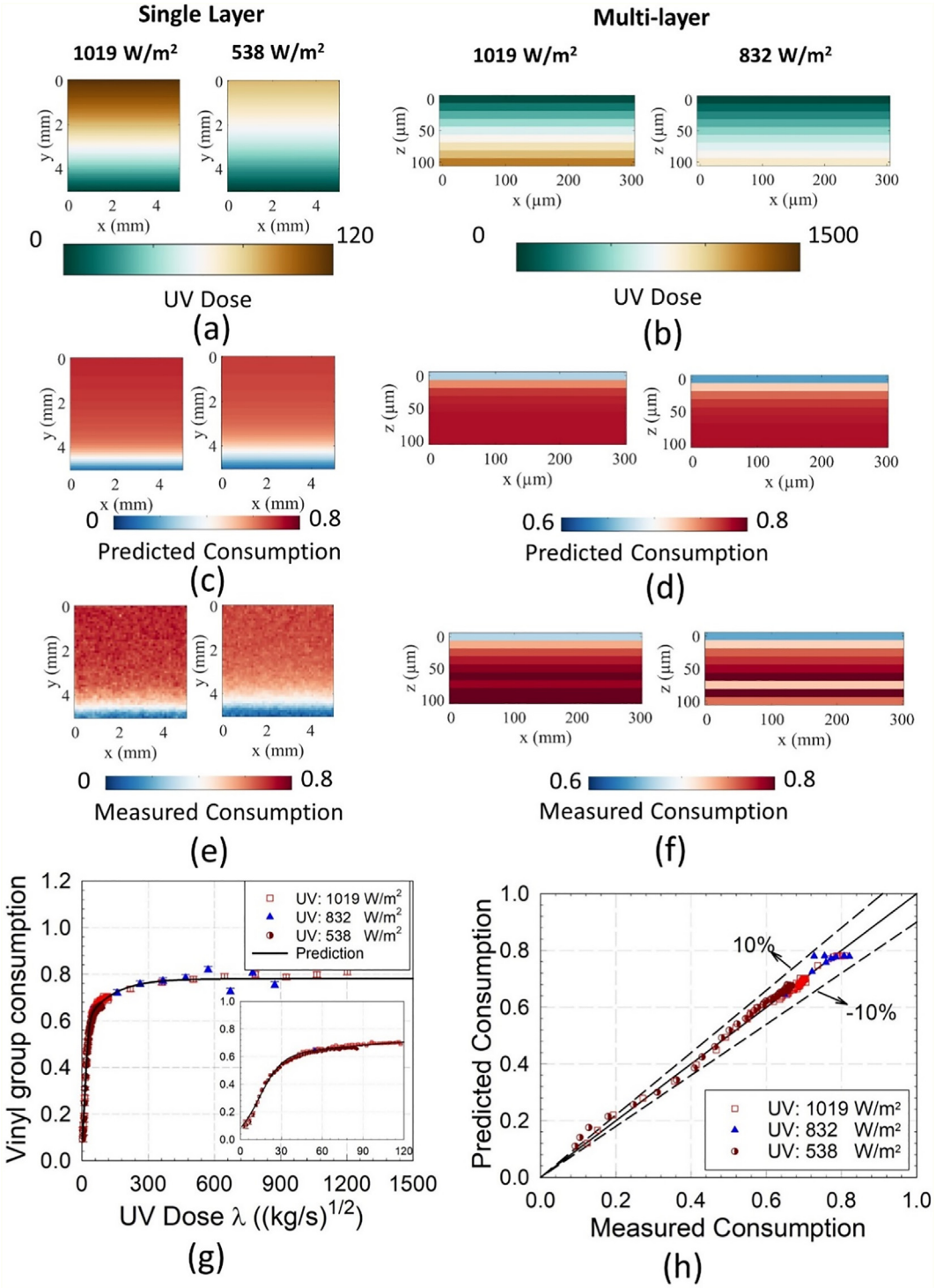

Fig. 3. Validation of the established model by using single layer and multilayer samples printed under a range of different UV intensities: **a)** calculated distribution of UV radiation dose in a single layer; **b)** calculated distribution of UV radiation dose through multilayers; **c)** predicted distribution of vinyl group consumption in a single layer; **d)** predicted distribution of vinyl group consumption through multilayers; **e)** measured distribution of vinyl group consumption in a single layer; **f)** measured distribution of vinyl group consumption through multilayers; **g)** distribution of the experimental data points of vinyl group consumption in comparison with the prediction curve; **h)** deviation assessment experiment data versus prediction.

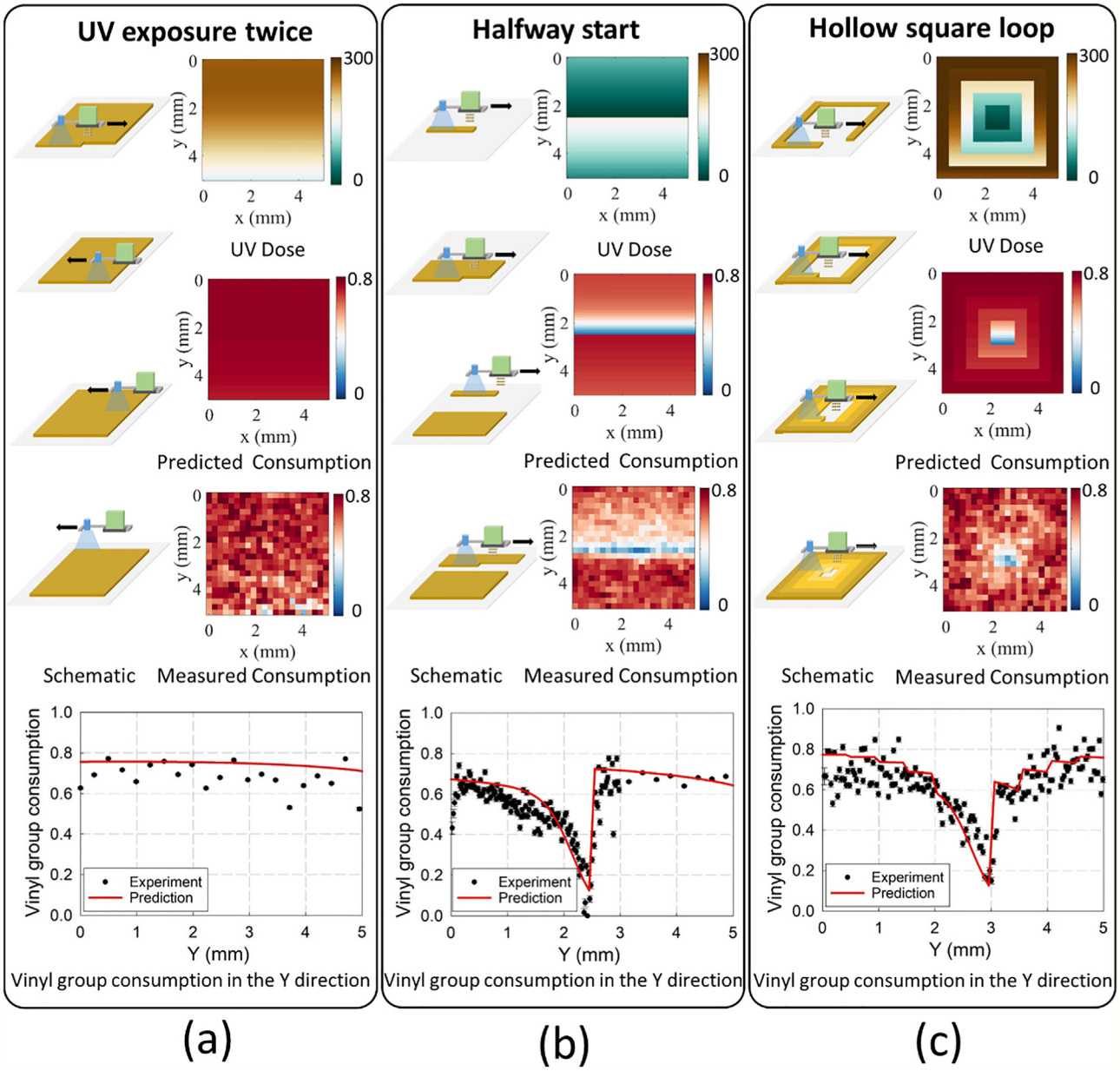

Fig. 4. Demonstration of optimising the printing strategy with the established model's help to address existing printing defect in the standard strategy: prediction and validation of vinyl group consumption in three designed printing strategies **a)** UV exposure twice; **b)** halfway start; **c)** hollow square loop.

expected for a fully cured diacrylate [48,50]. The amount of UV dose received by the bottom layer ($1328.63(kg/s)^{1/2}$) was more than ten times higher than that of the top layer ($82.79(kg/s)^{1/2}$), which is shown in Fig. 2d.

The relationship between UV radiation dose and degree of vinyl group consumption of both single layer and multilayer inkjet printing under the UV intensity 1245 W/m^2 is shown in Fig. 2e. The consumption starts with a sharp increase when UV is applied, followed by a plateau stage where the consumption is relatively stable, despite further UV dosing. The sharp increase in the consumption of the vinyl groups is consistent with efficient initiation, based on the choice of initiator and good penetration of the UV energy. The plateau is hypothesised to be a result of the process becoming mass and heat transfer limited, as the local viscosity increases with conversion to the polymer. The vinyl group consumption is 0.7 at the UV radiation dose of $130(\mathrm{kg/s})^{1/2}$. However, the degree of vinyl group consumption only reaches 0.78 when the UV radiation dose is five to ten times of this dose. Similar phenomena have been observed in the literature. For a diacrylate monomer, the vinyl group consumption limit was around 80% [48,50]. This indicates that we are close to full monomer consumption with UV doses of $130(\mathrm{kg/s})^{1/2}$.

The data points in Fig. 2e consist of a combination of single layer and multilayer measurements. The experimental degree of vinyl group consumption versus calculated UV radiation dose under UV intensity 1245 W/m^2 can be fitted by the proposed correlation (Eq. (17)) with a coefficient of determination$R^2 = 0.99$. The experimentally fitted parameters for Eq. (17) (Fig. 2e) are shown in Table 1,

Fig. 2f compares the variation between the measured degree of vinyl group consumption distribution and predictions calculated by Eq. (17). There is a good agreement between the predictions and the experiments, with about 95% of data points within 5%

error, and the agreement level is the lowest for two points at lower values of degree of vinyl group consumption (15.8% error at the consumption of 0.15 and 6% errors at the consumption of 0.12). Experimental measurement errors, including excessive film spreading and oxygen inhibition [66], are likely to cause the overestimation of the degree of vinyl group consumption in this case.

To validate the feasibility of the correlation (Eq. (17)) and fitted parameters (Table 1) in the application of a wide range of UV light intensities, samples printed at different UV intensities were characterised. Fig. 3a-f shows the calculated UV radiation dose and predicted and measured degrees of vinyl group consumption under different UV light intensities. Comparison of predicted UV radiation dose and measured degree of vinyl group consumption is shown in Supplementary Section 8. Single layer inkjet printing (Fig. 3a, 3c and 3e) showed that the UV radiation dose was constant in the X-direction and decreased in the Y-direction from the starting point. For the multilayer inkjet printed samples (Fig. 3b, 3d and 3f), it was found that there was little vinyl group consumption difference in Z except for the top two layers ($\sim 20\mu$m), even when the UV intensity had 25% difference (1019 W/m^2 and 832 W/m^2). The results also show that, no matter how much the UV radiation dose increases, the degree of vinyl group consumption did not change for the bottom three layers, which is because they had reached the expected maximum vinyl group consumption that is achievable with a difunctional monomer. Fig. 3g and h show that the proposed correlation (Eq. (17)) matches well with the measured data for the degree of vinyl group consumption, with deviation below 10%. The level of agreement decreases somewhat at the lower degrees of vinyl group consumption (<0.2), as noted previously.

3.2. Utilising the model to design an optimal printing strategy

The predictive model established in this work can be used to construct the unreacted vinyl group distribution map in an inkjet printed structure. This can help the user to predict potential sample defects as well as to optimise printing strategies to address them. For example, by analysing the distribution of vinyl group on the printed layer, we found the lowest degrees of vinyl group consumption (0.12) appeared at the bottom edge of the printed sample (Fig. 2a and 3e). This effect was likely caused by insufficient UV radiation for the last few swathes and leads to a sagging effect, which has been reported in previous studies [16,18,67]. This can also causes product qualitity problems for example, when manufacturing personalized pharmaceutical and healthcare devices [68], an insufficient cure can lead to unreacted chemical residuals that could leach out during application. These ink residuls can cause allergic effects, irritation, or inflammatory response of the surrounding tissue in both the short and long term [69]. We chose three printing strategies (Fig. 4) that are achievable with our printer to potentially address the problems discussed above.

1. UV exposure twice (Fig. 4a): After finishing a standard printing process, the UV source re-scans, this time from the endpoint to the start printing point. The UV dose at each element with this printing strategy significantly increases compared with the standard printing strategy.
2. Halfway start (Fig. 4b): this strategy divides the target square into upper and lower halves. The print begins from the middle of the square to complete the lower half first, and then the upper half is printed. This strategy moves the lower UV dose section to the centre and therefore minimized the sagging effect.
3. Hollow square loop (Fig. 4c): To create a barrier at the beginning of each layer to minimise the sagging effect, hollow squares were printed repeatedly from the outer to the inner until all space was covered.

By comparing the predictive data with experimental measurement (Fig. 4a, b and c), we demonstrate that our predictive model is qualified for validating printing strategies without the need to carry out an actual experiment. This will help the user to accelerate the product quality optimisation process with minimum effort and cost. In addition, we choose squares for simplicity of analysis where complex patterns are also applicable (Supplementary Section 13). The predictive model and design framework developed in this study work in different applications regardless of the printing resolution or shapes. The UV pinning technique used in this study can help improve the manufacturing accuracy, especially when printing fine patterns. However, even by using the UV pinning inkjet fine resolution technique, we still noticed a loss of manufacturing quality at the bottom end of each layer due to the sagging effect of the less cured ink [16]. The under-cured bottom edge is unavoidable during the standard UV pinning inkjet printing strategy, while the proposed design framework can be used to optimise printing and minimise the resulting poor print geometry.

Besides product quality, the building time of different printing strategies is also a factor that should be considered. We, therefore, introduce a manufacturing time model (Section 2.5 and Supplementary Section 9) to help further evaluate the efficiency of a chosen strategy (Fig. 5).

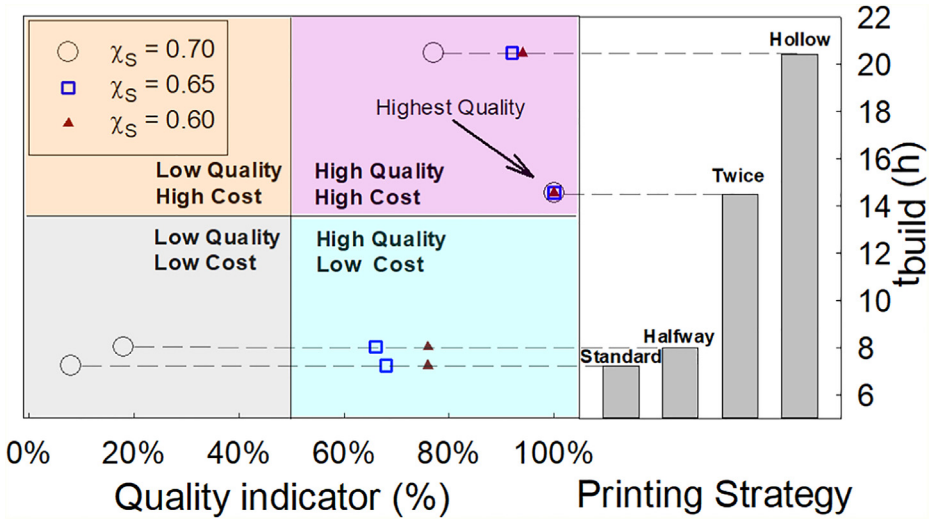

Fig. 5. Quality indicator vs. build time per 100 samples for different χ_s (user-determined threshold of the degree of vinyl group consumption).

To avoid experimental error, predicted results were used rather than experimental data to calculate the quality indicator of four different printing strategies. Here we define a 100% quality indicator when all the elements of the sample achieve the user-determined quality threshold (χ_s). The highest quality (i.e. 100%) is always achieved when applying the 'UV exposure twice' strategy. However, this strategy is very time-consuming, so only when a high level of ink polymerisation is required does it become the best choice when considering time and cost. When such quality (100%) is not necessary, the build time can significantly be reduced, and the halfway start and standard strategies become competitive, providing $\sim 80\%$ quality with only $\sim 50\%$ build time (cost). It can therefore be seen that selecting the user-determined threshold will affect the quality indicator, which can then lead to a different optimal scan strategy when time and cost of manufacturing are also considered. Significantly, it is clearly demonstrated that the evaluation methodology presented in this work can accurately predict build quality and time. This methodology can be used as a simple but powerful aid to determine the best commercial decision when designing printing strategies.

4. Conclusions

In this study, a systematic investigation of UV curing in inkjet printing was conducted by a combined experimental and modelling study to understand the effect of UV illumination conditions and printing strategies on the degree of vinyl group consumption achieved during inkjet printing. A novel descriptive model and a highly accurate predictive model for UV based inkjet printing of polymeric materials were both developed and validated. These models allowed printing strategies to be designed that deliver the optimum print process by balancing the technical (quality of product), environmental (reduced waste/scrap and commercial (performance fit application) demands, dependent on the end-user's specifications. The modelling approach was shown to have the capability to predict the degree of vinyl group consumption both spatially and temporally, which in turn enabled the end-user to make the best commercial and environmental decision, so preventing over or under the engineering of the final inkjet article. To do this, the model considered the processing parameters, including UV source pathway, intensity, spatial distribution, and interlayer attenuation. The model was verified and validated via experimental work that demonstrated that vinyl group consumption could be correlated with the amount of UV received. Moreover, a novel design framework was developed based on the proposed model to help the user optimise the printing strategy efficiently, economically and environmentally, only requiring a limited number of experiments. A design demonstration showed the performance of the optimised printing strategy could be significantly improved by the application of the model. This study shows good application prospects for designing and optimising inkjet printing with the free radical photopolymerisation process in scientific research and industrial applications.

CRediT authorship contribution statement

Peng Zhao: Methodology, Software, Formal analysis, Writing - original draft, Visualization. **Yinfeng He:** Methodology, Validation, Investigation, Writing - original draft, Visualization. **Gustavo F. Trindade:** Methodology, Investigation, Writing - original draft, Visualization. **Martin Baumers:** Methodology, Writing - review & editing. **Derek J. Irvine:** Methodology, Writing - review & editing, Funding acquisition. **Richard J.M. Hague:** Conceptualization, Project administration, Funding acquisition. **Ian A. Ashcroft:** Conceptualization, Writing - review & editing, Project administration, Funding acquisition, Supervision. **Ricky D. Wildman:** Conceptualization, Writing - review & editing, Project administration, Funding acquisition, Supervision.

Declaration of Competing Interest

The author declare that there is no conflict of interest.

Acknowledgements

This work was supported by the Engineering and Physical Sciences Research Council [grant nos. EP/N024818/1 and EP/P031684/1], funded at the University of Nottingham.. The authors would also like to acknowledge the access to the confocal Raman microscopy facility at the Nanoscale and Microscale Research Centre (nmRC) of the University of Nottingham with support from Dr Graham Rance.

Appendix A. Supplementary data

Supplementary data to this article can be found online at https://doi.org/10.1016/j.matdes.2021.109889.

References

[1] E. Saleh, F. Zhang, Y. He, J. Vaithilingam, J.L. Fernandez, R. Wildman, I. Ashcroft, R. Hague, P. Dickens, C. Tuck, 3D Inkjet printing of electronics using UV conversion, Adv. Mater. Technol. 2 (2017), https://doi.org/10.1002/admt.201700134.
[2] E. Saleh, P. Woolliams, B. Clarke, A. Gregory, S. Greedy, C. Smartt, R. Wildman, I. Ashcroft, R. Hague, P. Dickens, C. Tuck, 3D inkjet-printed UV-curable inks for multi-functional electromagnetic applications, Addit. Manuf. 13 (2017) 143–148, https://doi.org/10.1016/j.addma.2016.10.002.
[3] D.J. Hayes, W.R. Cox, M.E. Grove, Micro-jet printing of polymers and solder for electronics manufacturing, J. Electron. Manuf. 8 (1998) 209–216, https://doi.org/10.1142/s0960313198000197.
[4] Y. Wang, H. Guo, J.J. Chen, E. Sowade, Y. Wang, K. Liang, K. Marcus, R.R. Baumann, Z.S. Feng, Paper-based inkjet-printed flexible electronic circuits, ACS Appl. Mater. Interfaces. 8 (2016) 26112–26118, https://doi.org/10.1021/acsami.6b06704.
[5] D. Ju, T. Zhang, J. Xiao, X. Qiao, Z. Huang, Effect of droplet sizes on evaporation of a bi-component droplet at DME (dimethyl ether)/n-heptane-fueled engine conditions, Energy. 86 (2015) 257–266, https://doi.org/10.1016/j.energy.2015.04.030.
[6] F. Zhang, E. Saleh, J. Vaithilingam, Y. Li, C.J. Tuck, R.J.M. Hague, R.D. Wildman, Y. He, Reactive material jetting of polyimide insulators for complex circuit board design, Addit. Manuf. 25 (2019) 477–484, https://doi.org/10.1016/j.addma.2018.11.017.
[7] E.M. Hamad, S.E.R. Bilatto, N.Y. Adly, D.S. Correa, B. Wolfrum, M.J. Schöning, A. Offenhäusser, A. Yakushenko, Inkjet printing of UV-curable adhesive and dielectric inks for microfluidic devices, Lab Chip. 16 (2016) 70–74, https://doi.org/10.1039/c5lc01195g.
[8] R. Daly, T.S. Harrington, G.D. Martin, I.M. Hutchings, Inkjet printing for pharmaceutics – a review of research and manufacturing, Int. J. Pharm. 494 (2015) 554–567, https://doi.org/10.1016/j.ijpharm.2015.03.017.
[9] E.A. Clark, M.R. Alexander, D.J. Irvine, C.J. Roberts, M.J. Wallace, S. Sharpe, J. Yoo, R.J.M. Hague, C.J. Tuck, R.D. Wildman, 3D printing of tablets using inkjet with UV photoinitiation, Int. J. Pharm. 529 (2017) 523–530, https://doi.org/10.1016/j.ijpharm.2017.06.085.
[10] Y. He, R. Foralosso, G.F. Trindade, A. Ilchev, L. Ruiz-Cantu, E.A. Clark, S. Khaled, R.J.M. Hague, C.J. Tuck, F.R.A.J. Rose, G. Mantovani, D.J. Irvine, C.J. Roberts, R.D. Wildman, A reactive prodrug ink formulation strategy for Inkjet 3D printing of controlled release dosage forms and implants, Adv. Ther. (2020) 1900187, https://doi.org/10.1002/adtp.201900187.
[11] T. Xu, W. Zhao, J.M. Zhu, M.Z. Albanna, J.J. Yoo, A. Atala, Complex heterogeneous tissue constructs containing multiple cell types prepared by inkjet printing technology, Biomaterials. 34 (2013) 130–139, https://doi.org/10.1016/j.biomaterials.2012.09.035.
[12] K. Arai, S. Iwanaga, H. Toda, C. Genci, Y. Nishiyama, M. Nakamura, Three-dimensional inkjet biofabrication based on designed images, Biofabrication. 3 (2011), https://doi.org/10.1088/1758-5082/3/3/034113 034113.
[13] P. Hubert, T. Centea, L. Grunefelder, S. Nutt, J. Kratz, A. Levy, Out-of-autoclave prepreg processing, in: Compr. Compos. Mater. II, Elsevier, 2017: pp. 63–94. https://doi.org/10.1016/B978-0-12-803581-8.09900-8.
[14] J.H. Jorge, E.T. Giampaolo, A.L. Machado, C.E. Vergani, Cytotoxicity of denture base acrylic resins: a literature review, J. Prosthet. Dent. 90 (2003) 190–193, https://doi.org/10.1016/S0022-3913(03)00349-4.

[15] Y. Hayran, Y. Keskin, S. Yilmaz, Cytotoxicity of polymethylmethacrylate copolymers, Ann. Med. Res. 26 (2019) 1868, https://doi.org/10.5455/annalsmedres.2019.06.335.
[16] Y. He, C.J. Tuck, E. Prina, S. Kilsby, S.D.R. Christie, S. Edmondson, R.J.M. Hague, F. R.A.J. Rose, R.D. Wildman, A new photocrosslinkable polycaprolactone-based ink for three-dimensional inkjet printing, J. Biomed. Mater. Res. - Part B Appl. Biomater. 105 (2017) 1645–1657, https://doi.org/10.1002/jbm.b.33699.
[17] X. Chen, I.A. Ashcroft, C.J. Tuck, Y.F. He, R.J.M. Hague, R.D. Wildman, An investigation into the depth and time dependent behavior of UV cured 3D ink jet printed objects, J. Mater. Res. 32 (2017) 1407–1420, https://doi.org/10.1557/jmr.2017.4.
[18] Y. He, F. Zhang, E. Saleh, J. Vaithilingam, N. Aboulkhair, B. Begines, C.J. Tuck, R.J. M. Hague, I.A. Ashcroft, R.D. Wildman, A tripropylene glycol diacrylate-based polymeric support ink for material jetting, Addit. Manuf. 16 (2017) 153–161, https://doi.org/10.1016/j.addma.2017.06.001.
[19] Y. He, R.D. Wildman, C.J. Tuck, S.D.R. Christie, S. Edmondson, An investigation of the behavior of solvent based polycaprolactone ink for material jetting, Sci. Rep. (2016), https://doi.org/10.1038/srep20852.
[20] Y. He, S. Kilsby, C. Tuck, R. Wildman, S. Christie, S. Edmonson, H. Yang, Processing biodegradable polycaprolactone through 3D printing, in: 24th Int. SFF Symp. - An Addit. Manuf. Conf. SFF 2013, 2013.
[21] X. Li, R. Chen, Y. Zhao, Q. Liu, J. Liu, J. Yu, J. Li, P. Liu, J. Li, J. Wang, Layer-by-layer inkjet printing GO film anchored Ni(OH)2 nanoflakes for high-performance supercapacitors, Chem. Eng. J. (2019), https://doi.org/10.1016/j.cej.2019.121988.
[22] W.J. Shin, H. Lee, Y. Sohn, W.G. Shin, Novel inkjet droplet method generating monodisperse hollow metal oxide micro-spheres, Chem. Eng. J. (2016), https://doi.org/10.1016/j.cej.2016.02.021.
[23] Y. Gu, A. Wu, J.F. Federici, X. Zhang, Inkjet printable constantan ink for the fabrication of flexible and conductive film, Chem. Eng. J. (2017), https://doi.org/10.1016/j.cej.2016.12.071.
[24] G.F. Trindade, F. Wang, J. Im, Y. He, A. Balogh, D. Scurr, I. Gilmore, M. Tiddia, E. Saleh, D. Pervan, L. Turyanska, C.J. Tuck, R. Wildman, R. Hague, C.J. Roberts, Residual polymer stabiliser causes anisotropic electrical conductivity during inkjet printing of metal nanoparticles, Commun. Mater. 2 (2021) 47, https://doi.org/10.1038/s43246-021-00151-0.
[25] J.R. Sheats, J.J. Diamond, J.M. Smith, Photochemistry in strongly absorbing media, J. Phys. Chem. 92 (1988) 4922–4938, https://doi.org/10.1021/j100328a023.
[26] J.H. Lee, R.K. Prud'homme, I.A. Aksay, Cure depth in photopolymerization: Experiments and theory, J. Mater. Res. (2001), https://doi.org/10.1557/JMR.2001.0485.
[27] L. Lecamp, P. Lebaudy, B. Youssef, C. Bunel, Influence of UV radiation wavelength on conversion and temperature distribution profiles within dimethacrylate thick material during photopolymerization, Polymer (Guildf). 42 (2001) 8541–8547, https://doi.org/10.1016/S0032-3861(01)00353-6.
[28] G. Tourloukis, S. Stoyanov, T. Tilford, C. Bailey, Predictive modelling for 3D inkjet printing processes, Proc. Int. Spring Semin. Electron. Technol. (2016), https://doi.org/10.1109/ISSE.2016.7563201.
[29] J.J. Karnes, T.H. Weisgraber, J.S. Oakdale, M. Mettry, M. Shusteff, J. Biener, On the network topology of cross-linked acrylate photopolymers: a molecular dynamics case study, J. Phys. Chem. B. 124 (2020) 9204–9215, https://doi.org/10.1021/acs.jpcb.0c05319.
[30] J. Lalevée, F. Morlet-Savary, C. Dietlin, B. Graff, J.P. Fouassier, Photochemistry and radical chemistry under low intensity visible light sources: application to photopolymerization reactions, Molecules. 19 (2014) 15026–15041, https://doi.org/10.3390/molecules190915026.
[31] P. Sanjuan-Alberte, J. Vaithilingam, J.C. Moore, R.D. Wildman, C.J. Tuck, M.R. Alexander, R.J.M. Hague, F.J. Rawson, Development of conductive gelatine-methacrylate inks for two-photon polymerisation, Polymers (Basel). 13 (2021) 1038, https://doi.org/10.3390/polym13071038.
[32] X. Xu, A. Awad, P. Robles-Martinez, S. Gaisford, A. Goyanes, A.W. Basit, Vat photopolymerization 3D printing for advanced drug delivery and medical device applications, J. Control. Release. 329 (2021) 743–757, https://doi.org/10.1016/j.jconrel.2020.10.008.
[33] C.K. Chua, S.M. Chou, T.S. Wong, A study of the state-of-the-art rapid prototyping technologies, Int. J. Adv. Manuf. Technol. 14 (1998) 146–152, https://doi.org/10.1007/BF01322222.
[34] M.M. Emami, D.W. Rosen, Modeling of light field effect in deep vat polymerization for grayscale lithography application, Addit. Manuf. 36 (2020), https://doi.org/10.1016/j.addma.2020.101595 101595.
[35] Y. Li, Q. Mao, J. Yin, Y. Wang, J. Fu, Y. Huang, Theoretical prediction and experimental validation of the digital light processing (DLP) working curve for photocurable materials, Addit. Manuf. 37 (2021), https://doi.org/10.1016/j.addma.2020.101716 101716.
[36] M. Srinivas, B.S. Babu, A Critical Review on Recent Research Methodologies in Additive Manufacturing, in: Mater. Today Proc., Elsevier Ltd, 2017: pp. 9049–9059. https://doi.org/10.1016/j.matpr.2017.07.258.
[37] M. Shusteff, A.E.M. Browar, B.E. Kelly, J. Henriksson, T.H. Weisgraber, R.M. Panas, N.X. Fang, C.M. Spadaccini, One-step volumetric additive manufacturing of complex polymer structures, Sci. Adv. 3 (2017) eaao5496, https://doi.org/10.1126/sciadv.aao5496.
[38] S. Westbeek, J.J.C. Remmers, J.A.W. van Dommelen, H.H. Maalderink, M.G.D. Geers, Prediction of the deformed geometry of vat photo-polymerized components using a multi-physical modeling framework, Addit. Manuf. 40 (2021), https://doi.org/10.1016/j.addma.2021.101922 101922.
[39] A. Wagner, A.M. Kreuzer, L. Göpperl, L. Schranzhofer, C. Paulik, Foamable acrylic based ink for the production of light weight parts by inkjet-based 3D printing, Eur. Polym. J. 115 (2019) 325–334, https://doi.org/10.1016/j.eurpolymj.2019.03.031.
[40] G. Yang, S. Peng, A. Ridyard, J. Kuta, UV LED curing in inkjet printing applications, in: Int. Conf. Digit. Print. Technol., Society for Imaging Science and Technology, 2008: pp. 535–537.
[41] V. Jašo, D. Stoiljković, R. Radičević, O. Bera, Kinetic modeling of bulk free-radical polymerization of methyl methacrylate, Polym. J. (2013), https://doi.org/10.1038/pj.2013.6.
[42] J.M. Liu, Simple technique for measurements of pulsed Gaussian-beam spot sizes, Opt. Lett. 7 (1982) 196, https://doi.org/10.1364/ol.7.000196.
[43] J. Blazej, The measurement of a transverse profile of laser beam by Knife Edge method, Http://People.Fjfi.Cvut.Cz/Blazejos/Public/Ul7En.Pdf. 52 (2013) 3–8. http://people.fjfi.cvut.cz/blazejos/public/ul7en.pdf (accessed November 18, 2019).
[44] D.F. Swinehart, The Beer-Lambert Law, J. Chem. Educ. 39 (1962) 333, https://doi.org/10.1021/ed039p333.
[45] G. Odian, Principles of Polymerization, John Wiley & Sons, Inc., 2004. https://doi.org/10.1002/047147875x.
[46] W.-F. Su, Principles of polymer design and synthesis, Extracts. (2013), https://doi.org/10.1007/978-3-642-38730-2.
[47] G.A. O'Neil, J.M. Torkelson, Modeling insight into the diffusion-limited cause of the gel effect in free radical polymerization, Macromolecules (1999), https://doi.org/10.1021/ma9811324.
[48] C. Patacz, X. Coqueret, C. Decker, Electron-beam initiated polymerization of acrylate compositions 3: Compared reactivity of hexanediol and tripropyleneglycol diacrylates under UV or EB initiation, Radiat. Phys. Chem. (2001), https://doi.org/10.1016/S0969-806X(01)00209-2.
[49] D.L. Kurdikar, N.A. Peppas, A kinetic study of diacrylate photopolymerizations, Polymer (Guildf). 35 (1994) 1004–1011, https://doi.org/10.1016/0032-3861(94)90945-8.
[50] F. Jiang, D. Drummer, Curing kinetic analysis of acrylate photopolymer for additive manufacturing by photo-DSC, Polymers (Basel). (2020), https://doi.org/10.3390/POLYM12051080.
[51] P. Rathi, S.J. Park, T. Kyu, Effects of photointensity gradient on directional crystal growth in blends of crystalline polymer and photoreactive monomer undergoing photopolymerization- induced phase transformation, J. Chem. Phys. 130 (2009), https://doi.org/10.1063/1.3126663.
[52] J. Simon, A. Langenscheidt, Curing behavior of a UV-curable inkjet ink: distinction between surface-cure and deep-cure performance, J. Appl. Polym. Sci. (2020), https://doi.org/10.1002/app.49218.
[53] E. Behroodi, H. Latifi, F. Najafi, A compact LED-based projection microstereolithography for producing 3D microstructures, Sci. Rep. (2019), https://doi.org/10.1038/s41598-019-56044-3.
[54] R. Liu, Y. Xu, J. Jia, P. Chen, F. Zhang, L. Zhang, Y. Chen, Improvement on curing performance and morphology of E51/TPGDA mixture in a free radical-cationic hybrid photopolymerization system, J. Polym. Res. 27 (2020) 1–10, https://doi.org/10.1007/s10965-020-02115-3.
[55] N.S. Kenning, B.A. Ficek, C.C. Hoppe, A.B. Scranton, Spatial and temporal evolution of the photoinitiation rate for thick polymer systems illuminated by polychromatic light: Selection of efficient photoinitiators for LED or mercury lamps, Polym. Int. (2008), https://doi.org/10.1002/pi.2455.
[56] M. Baumers, P. Dickens, C. Tuck, R. Hague, The cost of additive manufacturing: machine productivity, economies of scale and technology-push, Technol. Forecast. Soc. Change. (2016), https://doi.org/10.1016/j.techfore.2015.02.015.
[57] M. Baumers, Economic aspects of additive manufacturing: benefits, costs and energy consumption, Dr. Thesis, Loughbrgh. Univ. (2012), https://doi.org/10.1007/s13398-014-0173-7.2.
[58] J. Ding, M. Baumers, E.A. Clark, R.D. Wildman, The economics of additive manufacturing: towards a general cost model including process failure, Int. J. Prod. Econ. (2021), https://doi.org/10.1016/j.ijpe.2021.108087 108087.
[59] B.M. Colosimo, S. Cavalli, M. Grasso, A cost model for the economic evaluation of in-situ monitoring tools in metal additive manufacturing, Int. J. Prod. Econ. (2020), https://doi.org/10.1016/j.ijpe.2019.107532.
[60] Y. Yang, L. Li, Cost modeling and analysis for Mask Image Projection Stereolithography additive manufacturing: Simultaneous production with mixed geometries, Int. J. Prod. Econ. (2018), https://doi.org/10.1016/j.ijpe.2018.09.023.
[61] Y.P. Dong, J.C. Tang, D.W. Wang, N. Wang, Z.D. He, J. Li, D.P. Zhao, M. Yan, Additive manufacturing of pure Ti with superior mechanical performance, low cost, and biocompatibility for potential replacement of Ti-6Al-4V, Mater. Des. (2020), https://doi.org/10.1016/j.matdes.2020.109142.
[62] J. Xu, X. Gao, C. Zhang, S. Yin, Flax fiber-reinforced composite lattice cores: A low-cost and recyclable approach, Mater. Des. (2017), https://doi.org/10.1016/j.matdes.2017.07.066.
[63] Y. Yin, J. Zhang, Q. Tan, W. Zhuang, N. Mo, M. Bermingham, M.X. Zhang, Novel cost-effective Fe-based high entropy alloys with balanced strength and ductility, Mater. Des. (2019), https://doi.org/10.1016/j.matdes.2018.11.033.
[64] R. Tamura, T. Osada, K. Minagawa, T. Kohata, M. Hirosawa, K. Tsuda, K. Kawagishi, Machine learning-driven optimization in powder manufacturing of Ni-Co based superalloy, Mater. Des. (2020), https://doi.org/10.1016/j.matdes.2020.109290.
[65] H. Zhang, Y. Wu, K. Wang, Y. Peng, D. Wang, S. Yao, J. Wang, Materials selection of 3D-printed continuous carbon fiber reinforced composites considering

multiple criteria, Mater. Des. (2020), https://doi.org/10.1016/j.matdes.2020.109140.
[66] B.W. Brooks, Viscosity effects in free-radical polymerization of methyl methacrylate, Proc R Soc London Ser A. 357 (1977) 183–192, https://doi.org/10.1098/rspa.1977.0162.
[67] G.P. Hellmann, C. Kottlorz, J. Presser, K. Utaloff, Compact polymeric 3D prints of high stability, J. Mater. Res. (2014), https://doi.org/10.1557/jmr.2014.137.
[68] M.E. Prendergast, J.A. Burdick, Recent advances in enabling technologies in 3D printing for precision medicine, Adv. Mater. (2020), https://doi.org/10.1002/adma.201902516.
[69] S. Kamann, O. Aerts, L. Heinemann, Further evidence of severe allergic contact dermatitis from isobornyl acrylate while using a continuous glucose monitoring system, J. Diabetes Sci. Technol. (2018), https://doi.org/10.1177/1932296818762946.